NEGATIVE SHEAR LAG EFFECT IN CONTINUOUS DOUBLE T BEAM BY FEM

Dang-Bao TRAN[1,2], *Jaroslav NAVRÁTIL*[1]

[1] Department of Structures, Faculty of Civil Engineering, VSB–Technical University of Ostrava, Ludvíka Podéště 1875/17, Ostrava, Czech Republic.
[2] Department of Civil Engineering, Faculty of Architecture, Thu Dau Mot University, Tran Van On 06, Binh Duong Province, Vietnam.

dang.bao.tran@vsb.cz, jaroslav.navratil@vsb.cz

DOI: 10.35181/tces-2021-0005

Abstract. *This paper presents the use of a finite element method (FEM) to analyze the negative shear lag effect on prestressed continuous double T beam. However, the numerical method can be applied to i) any cross-section, ii). the most common types of supports, such as fixed, pinned, roller, iii) and any applied load, concentrated, or distributed passed through the shear center of the cross-section. The characteristics of the cross-section are firstly derived from 2D FEM, which uses a 9-node isoparametric element. Then, a 1D FEM, which uses a linear isoparametric element, is developed to compute the deflection, rotation angle, bending warping parameter, and stress resultants. Finally, the stress field is obtained from the local analysis on the 2D-cross section. A MATLAB program is executed to validate the numerical method.*

Keywords

Shear lag, restrained warping, prestressing, load, finite element method

1. Introduction

According to the elementary beam theory, when the beam element is under load, the longitudinal normal stresses are assumed to be proportional to the distance from the neutral axis. However, in practice, these stresses are nonuniformly distributed over the width of the cross-section. This phenomenon is called shear lag.

Many authors have researched the shear lag phenomenon. Reissner, E. [1] established a displacement field along the axis of the beam, taking into account the effect of shear lag, which is expressed by a parabolic function, and used the principle of minimum potential energy to obtain the flange stress at the cross-section. During the past several years, many authors [2-15] based on thinned wall beam theory [16] improved a spanwise displacement [1], which considers the warping of flanges, to analyze shear lag due to flexure. Most studies focus on concentrated and uniformly distributed loads. The effect of prestressed load on shear lag has only been performed in a few studies [7, 11]. Chang, S. T. [7] derived an analytical method from [2] and [1] to calculate the shear lag of simply supported prestressed concrete. Zhou, S. J. [11] proposed a new FEM to analyze the shear lag in prestressed concrete box girders.

The practical design of the beam structure requires faster and easier parameter adjustment than the 3D modelling using shell or solid. Some authors [17-21] have transformed the 3D analysis of the shear lag phenomenon into separated 2D cross-sectional and 1D modelling. El Fatmi, R. [17, 18] derived the nonuniform shear and torsional warping of arbitrary homogeneous cross-section from the Saint Venant beam problem extension. Le Corvec, V. and Filippou, F. C. [19] defined the axial displacement due to warping by interpolation a warping degrees of freedom number on the cross-section to establish FEM formulation for shear torsional warping in the elastic and elastoplastic analysis of beams. Ferradi, M.K. et al. [20] obtained FEM that accurately captures normal stress due to restrained warping by reproducing cross-sectional warping as a linear combination of warping modes. Dikaros, I. C. and Sapountzakis, E. J. [21] proposed a theory to determine nonuniform warping due to flexure of composite beam with arbitrary cross-section using the Boundary Element Method (BEM).

The purpose of this paper is to investigate the negative shear lag effect due to prestressing load in continuous double T beam by establishing a numerical method using FEM, based on displacement and strain fields derived from Dikaros, I. C. and Sapountzakis, E. J. [21]. A 2D FEM based on the Galerkin approach is obtained from computing the warping function of the corresponding elliptic differential equations. The other kinematical

variables of the beam are calculated from the principle of virtual work by developing a 1D FEM.

2. Formulation the problem

Let us consider a prismatic beam with arbitrary cross-section, constant along the length L, with modulus of elasticity E, and shear modulus G. The longitudinal axis is the x-axis, and the cross-sections lie in the y–z plane. The coordinate system is $Sxyz$ through the shear center of the cross-section S. $CXYZ$ is the parallel system with $Sxyz$ through the center of gravity C.

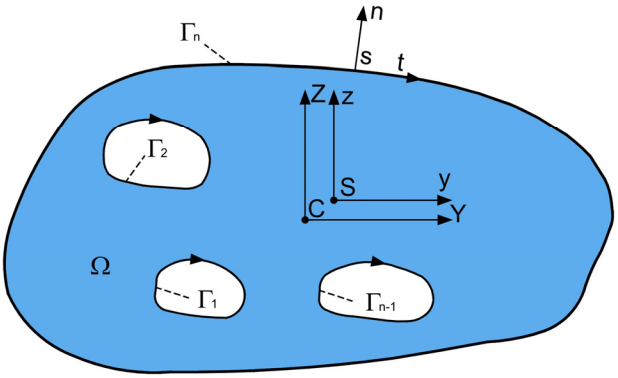

Fig. 1: Cross-section of a prismatic beam.

The multiply connected domain Ω is bounded by n curves, Γ_1, Γ_2, ..., Γ_{n-1}, Γ_n, as Fig. 1. Tangent vector **t** with associate coordinate s and normal vector **n** set up the right-handed system. The beam is exposed to the arbitrary distributed or concentrated loads, transverse loading $p_z(x)$ along the z-direction, bending moment $m_Y(x)$, and warping moment $m_{\varphi_{CY}^P}(x)$ along with the Y direction. The cross-section is assumed with no distortion.

The geometric constants of the beam are defined as

$$\begin{aligned} A &= \int_\Omega d\Omega, \\ I_{YY} &= \int_\Omega Z^2 d\Omega, \\ I_{ZZ} &= \int_\Omega Y^2 d\Omega, \\ I_{\varphi_{CY}^P \varphi_{CY}^P} &= \int_\Omega \varphi_{CY}^P \varphi_{CY}^P d\Omega, \end{aligned} \tag{1}$$

where A is the area of cross-section, I_{YY}, I_{ZZ} are the second moments of area with respect to Z, Y-axis, respectively, $I_{\varphi_{CY}^P \varphi_{CY}^P}$ is the warping constant.

φ_{CY}^P defines the shear warping function with respect to center of gravity C, which is obtained from

$$\varphi_{CY}^P = \phi_{CY}^P - Z, \tag{2}$$

where $\phi_{CY}^P(y,z)$ is determined from the elliptical differential equations

$$\begin{aligned} &\nabla^2 \phi_{CY}^P = -\left(\frac{A_Z^P}{I_{YY}}\right) Z \text{ in } \Omega \\ &\frac{\partial \phi_{CY}^P}{\partial y} n_y + \frac{\partial \phi_{CY}^P}{\partial z} n_z = 0 \text{ on } \Gamma_n, \end{aligned} \tag{3}$$

where $A_Z^P = k_Z A$ is defined as the primary shear area, k_Z is the shear correction factor obtained from the definition given in [22]

In addition, the evaluated warping function ϕ_{CY}^P from (3) contains an integration c^s, which can be obtained from Gruttmann, F. [23]

$$c^s = -\frac{1}{A}\int_\Omega \phi_{CY}^P dA. \tag{4}$$

The displacement field is expressed as [21]

$$\begin{aligned} \bar{u}(x,y,z) &= \bar{u}^P(x,y,z) + \bar{u}^S(x,y,z) \\ &= \theta_Y(x) Z + \eta_Y(x) \varphi_{CY}^P(y,z), \\ \bar{v}(x,y,z) &= 0, \\ \bar{w}(x,y,z) &= w(x), \end{aligned} \tag{5}$$

where $\bar{u}$, $\bar{v}$, $\bar{w}$ are the total displacements corresponding with the axis x, y, z

$\bar{u}^P$, $\bar{u}^S(x,y,z)$ are the primary and secondary axial displacement, respectively,

$\theta_Y(x)$ is the angle of rotation of the section about the Y axis,

η_Y is the bending warping parameter.

The stress field obtained from the theory of elasticity as [21]

$$\begin{aligned} \sigma_{xx} &= E\varepsilon_{xx} = \underbrace{E\theta_{Y,x} Z}_{\sigma_{xx}^P} + \underbrace{E\eta_{Y,x}\left(\varphi_{CY}^P\right)}_{\sigma_{xx}^S}, \\ \tau_{xy} &= G\gamma_{xy} = \underbrace{G\gamma_Z^P\left(Z_{,y} + \varphi_{CY,y}^P\right)}_{\tau_{xy}^P} + \underbrace{G\gamma_Z^S\left(\varphi_{CY,y}^P\right)}_{\tau_{xy}^S}, \\ \tau_{xz} &= G\gamma_{xz} = \underbrace{G\gamma_Z^P\left(Z_{,z} + \varphi_{CY,z}^P\right)}_{\tau_{xz}^P} + \underbrace{G\gamma_Z^S\left(\varphi_{CY,z}^P\right)}_{\tau_{xz}^S}, \end{aligned} \tag{6}$$

where $\gamma_Z^P = w_{,x} + \theta_Y$, $\gamma_Z^S = \eta_Y - w_{,x} - \theta_Y$ are defined as the primary and secondary shear strains, respectively. It is emphasized that the stress component σ_{xx} is composed of i) the classic normal stress, σ_{xx}^P, determined from the engineering beam theory and ii) the warping normal stress, σ_{xx}^S, caused by warping of the cross-section is the primary reason for the shear lag phenomenon.

The bending moment, the warping moment, the primary shear force, the secondary shear force are denoted M_Y, $M_{\varphi_{CY}^P}$, Q_z^P, Q_z^S, respectively obtained as [21]

$$\begin{aligned}
M_Y &= \int_\Omega \sigma_{xx} Z d\Omega = EI_{YY}\theta_{Y,x},\\
M_{\varphi_{CY}^P} &= \int_\Omega \sigma_{xx}\varphi_{CY}^P d\Omega = EI_{\varphi_{CY}^P\varphi_{CY}^P}\eta_{Y,x},\\
Q_Z^P &= \int_\Omega\left[\tau_{xy}\left(\phi_{CY,y}^P\right)+\tau_{xz}\left(\phi_{CY,z}^P\right)\right]d\Omega\\
&= G\gamma_Z^P\int_\Omega\left[\left(\phi_{CY,y}\right)^2+\left(\phi_{CY,z}\right)^2\right],\\
Q_Z^S &= \int_\Omega\left[\tau_{xy}\left(\varphi_{CY,y}^P\right)+\tau_{xz}\left(\varphi_{CY,z}^P\right)\right]d\Omega\\
&= -G\gamma_Z^S\int_\Omega\left[\left(\varphi_{CY,y}^P\right)^2+\left(\varphi_{CY,z}^P\right)^2\right]d\Omega.
\end{aligned} \tag{7}$$

3. FEM procedures

3.1. Deflection w_x, rotation angle θ_Y and bending warping parameter η_Y

The principle of virtual work ignoring volumetric forces is used to establish the stiffness matrix of the 1D beam element. Assume the beam element includes two end nodes, 1, 2, The symbol $\delta(.)$ denotes the virtual quantities. The internal virtual work is

$$W_i = \int_V\left(\sigma_{xx}\delta\varepsilon_{xx}+\tau_{xy}\delta\gamma_{xy}+\tau_{xz}\delta\gamma_{xz}\right)dV, \tag{8}$$

where V is the volume of a prismatic beam.

Substitution the Eq. (6) and Eq. (7) to Eq. (8), the internal virtual work can be rewritten as

$$\begin{aligned}
W_i = {} & EI_{YY}\int_0^L\delta\left(\theta_{Y,x}\right)\left(\theta_{Y,x}\right)dx + EI_{\varphi_{CY}^P\varphi_{CY}^P}\int_0^L\delta\left(\eta_{Y,x}\right)\eta_{Y,x}dx +\\
& GA_Z^P\int_0^L\delta\left(\gamma_Z^P\right)\left(\gamma_Z^P\right)dx + G(A-A_Z^P)\int_0^L\delta\left(\gamma_Z^S\right)\left(\gamma_Z^S\right)dx
\end{aligned} \tag{9}$$

The external virtual work is

$$\begin{aligned}
W_e = {} & \underbrace{\int_0^L\left(p_z(x)\delta w_x + m_Y\delta\theta_Y + m_{\varphi_{CY}^P}\delta\eta_Y\right)dx}_{Span} +\\
& \underbrace{\int_\Omega(t_x\delta\overline{u}+t_y\delta\overline{v}+t_z\delta\overline{w})d\Omega}_{end\ node,\ 1} + \underbrace{\int_\Omega(t_x\delta\overline{u}+t_y\delta\overline{v}+t_z\delta\overline{w})d\Omega}_{end\ node,\ 2},
\end{aligned} \tag{10}$$

where t_x, t_y, t_z are the components of traction vector applied on the lateral surface of the beam which is related to the end nodes- external loads as [21]

$$\begin{aligned}
&\hat{p}_z(x) = \int_\Omega t_z d\Omega,\ \ \hat{m}_Y(x) = \int_\Omega t_x Z d\Omega,\\
&\hat{m}_{(\varphi_{CY}^P)} = \int_\Omega t_x\varphi_{CY}^P d\Omega,
\end{aligned} \tag{11}$$

Using the expression Eq. (11), the Eq. (10) can be represented as

$$\begin{aligned}
W_e = {} & \int_0^L p_z(x)\delta w_x dx + \int_0^L m_Y\delta\theta_Y dx + \int_0^L m_{\varphi_{CY}^P}\delta\eta_Y dx +\\
& \sum_{i=1}^2\hat{p}_{zi}\delta w_{xi} + \sum_{i=1}^2\hat{m}_{Yi}\delta\theta_{Yi} + \sum_{i=1}^2\hat{m}_{\varphi_{CY}^P i}\delta\eta_{Yi}.
\end{aligned} \tag{12}$$

To derive the element stiffness matrix, the variables w_x, θ_Y, and η_Y need to be interpolated within each element. w_x, θ_Y and η_Y are independent variables. As a result, any kind of H^0 shape function can be used for the present beam. We use 1D linear isoparametric shape function for both variables [24, 25]. That is,

$$\begin{aligned}
w_x &= \left[N_1(\xi)\quad N_2(\xi)\right]\begin{Bmatrix}w_{x1}\\ w_{x2}\end{Bmatrix},\\
\theta_Y &= \left[N_1(\xi)\quad N_2(\xi)\right]\begin{Bmatrix}\theta_{Y1}\\ \theta_{Y2}\end{Bmatrix},\\
\eta_Y &= \left[N_1(\xi)\quad N_2(\xi)\right]\begin{Bmatrix}\eta_{Y1}\\ \eta_{Y2}\end{Bmatrix},
\end{aligned} \tag{13}$$

where w_{x1}, w_{x2}, θ_{Y1}, θ_{Y2}, η_{Y1}, η_{Y2} are the nodal displacements, rotation angle, bending warping parameter at the beam end nodes (1) and (2), respectively

$$N_1 = \frac{1}{2}(1-\xi),\ \ N_2 = \frac{1}{2}(1+\xi). \tag{14}$$

The corresponding element nodal degrees of freedom is $\mathbf{d} = \{w_{x1}, \theta_{Y1}, \eta_{Y1}, w_{x2}, \theta_{Y2}, \eta_{Y2}\}^T$. (15)

Substituting Eq. (13-14) to Eq. (9) and Eq. (12) leads to the element stiffness matrix and element force vector as

$$\mathbf{K}^e = \mathbf{K}_1^e + \mathbf{K}_2^e + \mathbf{K}_3^e + \mathbf{K}_4^e, \tag{16}$$

$$\mathbf{F}^e = \mathbf{F}_1^2 + \mathbf{F}_2^e + \mathbf{F}_3^e + \mathbf{F}_{i(p_z)}^e + \mathbf{F}_{i(m_Y)}^e + \mathbf{F}_{i(m_{\varphi_{CY}^P})}^e, \tag{17}$$

where

$$\mathbf{K}_1^e = EI_{YY}\int_{-1}^1\mathbf{B}_1^T\mathbf{B}_1 J d\xi = EI_{YY}\sum_i w_i\mathbf{B}_1^T\left(\xi_i\right)\mathbf{B}_1\left(\xi_i\right)J, \tag{18}$$

$$\begin{aligned}
\mathbf{K}_2^e &= EI_{\varphi_{CY}^P\varphi_{CY}^P}\int_{-1}^1\mathbf{B}_2^T\mathbf{B}_2 J d\xi\\
&= EI_{\varphi_{CY}^P\varphi_{CY}^P}\sum_i w_i\mathbf{B}_2^T\left(\xi_i\right)\mathbf{B}_2\left(\xi_i\right)J,
\end{aligned} \tag{19}$$

$$\begin{aligned}
\mathbf{K}_3^e &= GA_Z^P\int_{-1}^1\mathbf{B}_3^T\mathbf{B}_3 J d\xi\\
&= GA_Z^P\sum_i w_i\mathbf{B}_3^T\left(\xi_i\right)\mathbf{B}_3\left(\xi_i\right)J,
\end{aligned} \tag{20}$$

$$\mathbf{K}_4^e = G(A - A_Z^P)\int_{-1}^{1} \mathbf{B}_4^T \mathbf{B}_4 J d\xi = G(A - A_Z^P)\sum_i w_i \mathbf{B}_4^T(\xi_i)\mathbf{B}_4(\xi_i) J, \quad (21)$$

$$\mathbf{F}_1^e = \int_{-1}^{1} p_Z \mathbf{N}_1^T J d\xi = \sum_i w_i \mathbf{N}_1^T(\xi_i) p_Z J, \quad (22)$$

$$\mathbf{F}_2^e = \int_{-1}^{1} m_Y \mathbf{N}_2^T J d\xi = \sum_i w_i \mathbf{N}_2^T(\xi_i) m_Y J, \quad (23)$$

$$\mathbf{F}_3^e = \int_{-1}^{1} m_{\varphi_{CY}^P} \mathbf{N}_3^T J d\xi = \sum_i w_i \mathbf{N}_3^T(\xi_i) m_{\varphi_{CY}^P} J, \quad (24)$$

$\mathbf{F}_{i(p_z)}^e$, $\mathbf{F}_{i(m_Y)}^e$, $\mathbf{F}_{i(m_{\varphi_{CY}^P})}^e$ are the transverse forces, bending moments, warping moments at the end nodes i, respectively,

$$J = \frac{L}{2}, \quad (25)$$

$$\begin{aligned}
\mathbf{B}_1 &= \begin{bmatrix} 0 & N_{1,x} & 0 & 0 & N_{2,x} & 0 \end{bmatrix}, \\
\mathbf{B}_2 &= \begin{bmatrix} 0 & 0 & N_{1,x} & 0 & 0 & N_{2,x} \end{bmatrix}, \\
\mathbf{B}_3 &= \begin{bmatrix} N_{1,x} & N_1 & 0 & N_{2,x} & N_2 & 0 \end{bmatrix}, \\
\mathbf{B}_4 &= \begin{bmatrix} -N_{1,x} & -N_1 & N_1 & N_{2,x} & -N_2 & N_2 \end{bmatrix}, \\
\mathbf{N}_1 &= \begin{bmatrix} N_1 & 0 & 0 & N_2 & 0 & 0 \end{bmatrix}, \\
\mathbf{N}_2 &= \begin{bmatrix} 0 & N_1 & 0 & 0 & N_2 & 0 \end{bmatrix}, \\
\mathbf{N}_3 &= \begin{bmatrix} 0 & 0 & N_1 & 0 & 0 & N_2 \end{bmatrix},
\end{aligned} \quad (26)$$

w_i, ξ_i are the weights and the coordinate of integration points of the Gaussian integration technique. In the present study, to avoid the shear locking, we use one-point Gauss quadrature $(w_i = 2,\ \xi_i = 0)$.

Assembling the element stiffness matrix and load vectors in the system matrix equation given below

$$\mathbf{K}.\mathbf{d} = \mathbf{F}. \quad (27)$$

3.2. Warping function, ϕ_{CY}^P, φ_{CY}^P

Using Galerkin's method, with test function $\eta \in H^1(\Omega)$ and applying the Gauss-Green theorem, the governing equation (3) is transformed to weak form as

$$\int_\Omega \left(\frac{\partial \phi_{CY}^P}{\partial y}\frac{\partial \eta}{\partial y} + \frac{\partial \phi_{CY}^P}{\partial z}\frac{\partial \eta}{\partial z} \right) d\Omega - \int_\Omega \left(\frac{A_Z^P}{I_{YY}} \right) \eta \, d\Omega = 0. \quad (28)$$

The warping function value, ϕ_{CY}^P, in Eq. (28) is approximated by the FEM, which is presented in [22]. Finally, the value φ_{CY}^P is calculated from Eq. (2).

4. Validation example

In this section, a computer code is developed in the MATLAB R2015 based on the formulations described in the previous sections. A prestressed continuous beam with a double T cross-section was analyzed using this code. The beam's geometrical characteristics, the boundary and loading conditions are shown in Fig. 2.

Points B1, B2, and B3, are on the upper plate and have the y coordinates -1.55 m, -0.825 m, and 0, respectively. The straight tendons are positioned uniformly at the center of the slab. On the plan, tendons are arranged at the internal support with a total length of 2.8 m. Assume there are six tendons, each of which is stressed with a force of 140 kN. Modulus of elasticity E= 30 x 10^3 MPa, and the Poisson ratio ν = 0.2.

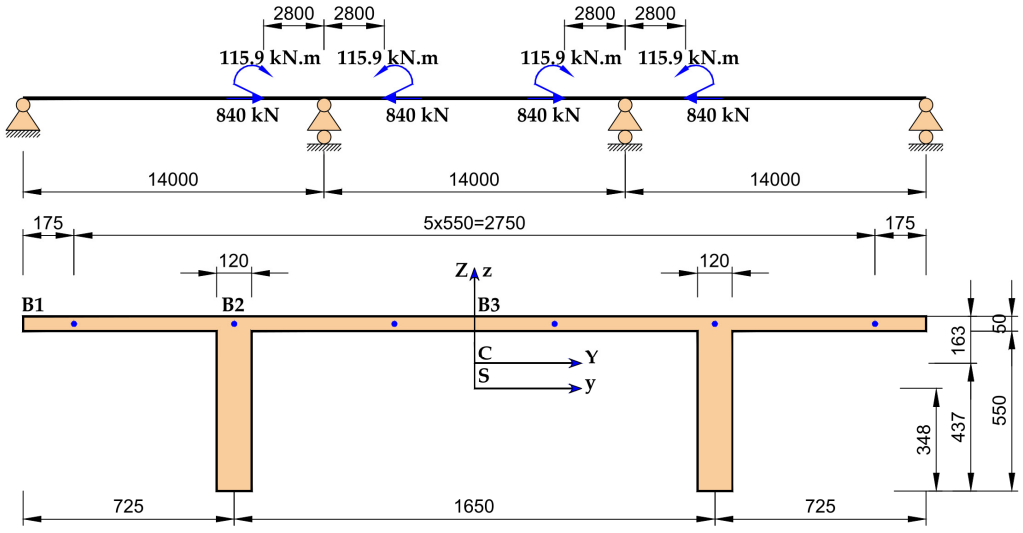

Fig. 2: Continuous beam, the load, and the geometry of the cross-section, units [mm].

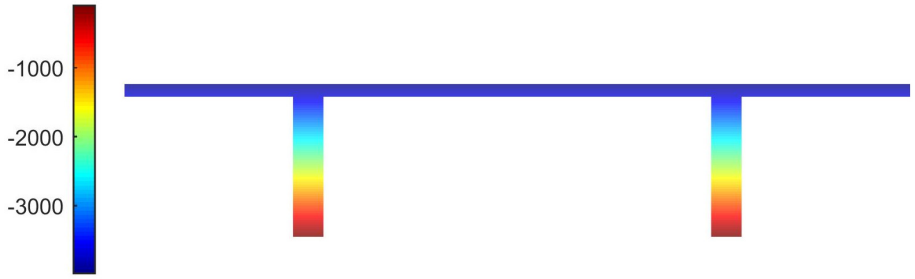

Fig. 3: The distribution of the classic normal stress in cross-section at x=14 m, units [kPa].

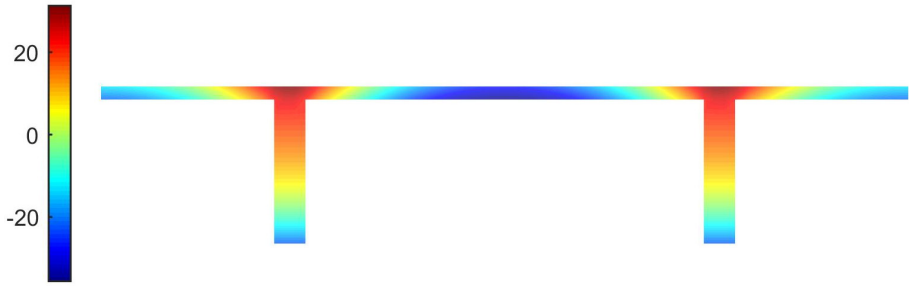

Fig. 4: The distribution of the warping normal stress in cross-section at x=14 m, units [kPa].

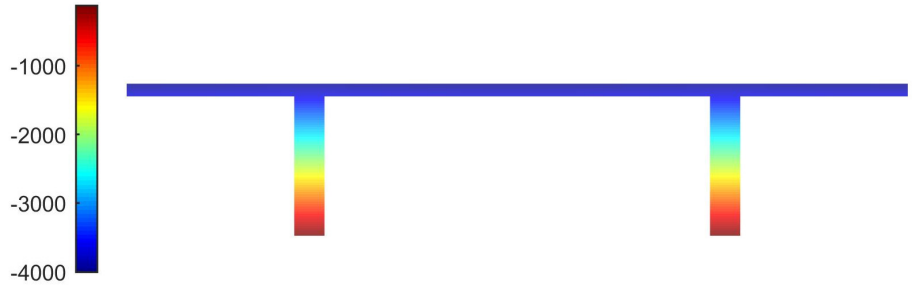

Fig. 5: The distribution of the total normal stress σ_{xx} in cross-section at x=14 m, units [kPa].

This example was analyzed by employing 840 axial elements and 126 elements in the cross-section. The geometric constant of the cross-section determined from the present study are as A= 0.287 m^2, k_Z = 0.2606, I_{YY} = 0.00977 m^4, $I_{\varphi_{CY}^P \varphi_{CY}^P}$ = 0.00248 m^4.

The prestressed load applied to the beam is transformed into two equivalent loads, P_x= 840 kN, and M_y= 115.9 kNm, shown in Fig 2. ETABS 2018 [26] is used to simulate 3D model included beam, shell, and tendon elements. The shell and beam elements are divided into 9856, 700 elements, respectively.

Fig. 3, Fig. 4, Fig.5 show the contour plot of the classic stress, the warping normal stress, and the total normal stress σ_{xx} on the cross-section predicted by the present study at the positions x= 14m, respectively. In Fig. 6, the variation of the total normal stress σ_{xx} along the width of the upper flange of the cross-section at the position x= 14 m is shown and compared between the result from i) Engineering beam theory, ii) 3D simulation ETABS 2018.

In Table 1, the normal stress σ_{xx} in the points B1, B2, and B3 predicted by the present study are given and compared with the results from 3D simulation. From the above Figures and Tables, the influence of the shear lag phenomenon is apparent, and the present study's accuracy can be verified.

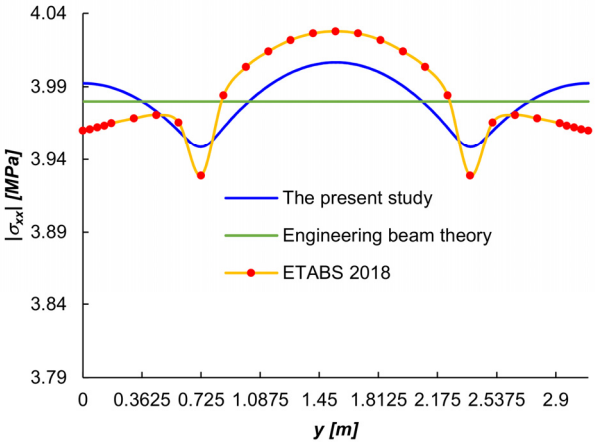

Fig. 6: The variation of the total normal stress σ_{xx} along the width in the upper flange at internal support.

Tab.1: Comparison of the normal stress σ_{xx} [MPa] at the points B1, B2, B3

Methods	Point B1	Point B2	Point B3
Present study	3.9924	3.9487	4.0066
ETABS 2018 [26]	3.96	3.93	4.025
Error (%)	0.818	0.475	0.457

5. Conclusions

In this paper, FEM is developed to analyze the negative shear lag effect due to prestressing in continuous double T beam. However, the numerical method can be used for arbitrary cross-sections with most boundary conditions and load types. A three-span continuous beam subjected to the prestressing load at the internal support was analyzed and compared with the results from 3D simulation software. It was observed that the present study could predict the negative shear lag phenomenon accurately due to prestressing load.

Acknowledgements

The works were supported by the Student Grant Competition VSB-TUO. The registration number of the project is SP2021/77 “Nonuniform torsion in prismatic beams with arbitrary cross-sections using FEM”

References

[1] REISSNER, E., 1946. Analysis of shear lag in box beams by the principle of minimum potential energy. *Quarterly of Applied Mathematics*. 1946. Vol. 4, no. 3, pp. 268–278. ISSN 0033-569X. DOI: 10.1090/qam/17176.

[2] CHANG, S. T. and F. Z. ZHENG, 1987. Negative Shear Lag in Cantilever Box Girder with Constant Depth. *Journal of Structural Engineering*. 1987. Vol. 113, no. 1, pp. 20–35. ISSN 0733-9445. DOI: 10.1061/(asce)0733-9445(1987)113:1(20).

[3] LUO, Q. Z., Q. S. LI and J. TANG, 2002. Shear lag in box girder bridges. *Journal of Bridge Engineering*. 2002. Vol. 7, no. 5, pp. 308–313. ISSN 1084-0702. DOI: 10.1061/(asce)1084-0702(2002)7:5(308).

[4] LUO, Q. Z., Y. M. WU, J. TANG and Q. S. LI, 2002. Experimental studies on shear lag of box girders. *Engineering Structures*. 2002. Vol. 24, no. 4, pp. 469–477. ISSN 01410296. DOI: 10.1016/S0141-0296(01)00113-4.

[5] ZHOU, S. J., 2010. Finite Beam Element Considering Shear-Lag Effect in Box Girder. *Journal of Engineering Mechanics*. 2010. Vol. 136, no. 9, pp. 1115–1122. ISSN 0733-9399. DOI: 10.1061/(asce)em.1943-7889.0000156.

[6] LUO, Q. Z., Y. M. WU, Q. S. LI, J. TANG and G. D. LIU, 2004. A finite segment model for shear lag analysis. *Engineering Structures*. 2004. Vol. 26, no. 14, pp. 2113–2124. ISSN 01410296. DOI: 10.1016/j.engstruct.2004.07.010.

[7] CHANG, S. T., 2004. Shear Lag Effect in Simply Supported Prestressed Concrete Box Girder. *Journal of Bridge Engineering*. 2004. Vol. 9, no. 2, pp. 178–184. ISSN 1084-0702. DOI: 10.1061/(asce)1084-0702(2004)9:2(178).

[8] LEE, S. C., C. H. YOO and D. Y. YOON, 2002. Analysis of Shear Lag Anomaly in Box Girders. *Journal of Structural Engineering*. 2002. Vol. 128, no. 11, pp. 1379–1386. ISSN 0733-9445. DOI: 10.1061/(asce)0733-9445(2002)128:11(1379).

[9] LUO, Q. Z., J. TANG and Q. S. LI, 2003. Shear lag analysis of beam-columns. *Engineering Structures*. 2003. Vol. 25, no. 9, pp. 1131–1138. ISSN 01410296. DOI: 10.1016/S0141-0296(03)00061-0.

[10] LIN, Z. and J. ZHAO, 2011. Least-work solutions of flange normal stresses in thin-walled flexural members with high-order polynomial. *Engineering Structures*. 2011. Vol. 33, no. 10, pp. 2754–2761. ISSN 01410296. DOI: 10.1016/j.engstruct.2011.05.022.

[11] ZHOU, S. J., 2011. Shear Lag Analysis in Prestressed Concrete Box Girders. *Journal of Bridge Engineering*. 2011. Vol. 16, no. 4, pp. 500–512. ISSN 1084-0702. DOI: 10.1061/(asce)be.1943-5592.0000179.

[12] QIN, X. X., H. B. LIU, S. J. WANG and Z. H. YAN, 2015. Symplectic Analysis of the Shear Lag Phenomenon in a T-Beam. *Journal of Engineering Mechanics*. 2015. Vol. 141, no. 5, pp. 04014157. ISSN 0733-9399. DOI: 10.1061/(asce)em.1943-7889.0000882.

[13] ZHANG, Y. H., 2012. Improved Finite-Segment Method for Analyzing Shear Lag Effect in Thin-Walled Box Girders. *Journal of Structural Engineering*. 2012. Vol. 138, no. 10, pp. 1279–1284. ISSN 0733-9445. DOI: 10.1061/(asce)st.1943-541x.0000552.

[14] ZHANG, Y. H. and L. X. LIN, 2014. Shear lag analysis of thin-walled box girders based on a new generalized displacement. *Engineering Structures*. 2014. Vol. 61, no. 4, pp. 73–83. ISSN 01410296. DOI: 10.1016/j.engstruct.2013.12.031.

[15] PROKIĆ, A., 2002. New finite element for analysis of shear lag. *Computers and Structures*. 2002. Vol. 80, no. 11, pp. 1011–1024. ISSN 00457949. DOI: 10.1016/S0045-7949(02)00036-6.

[16] VLASOV, V. Z., 1961. Thin walled elastic beams. Israel Program for Scientific Translations. *Jerusalem, Israel*. 1961.

[17] EL FATMI, R., 2007. Non-uniform warping including the effects of torsion and shear forces. Part I: A general beam theory. *International Journal of Solids and Structures*. 2007. Vol. 44, no. 18–19, pp. 5912–5929. ISSN 0020-7683. DOI: 10.1016/j.ijsolstr.2007.02.006.

[18] EL FATMI, R., 2007. Non-uniform warping including the effects of torsion and shear forces. Part II: Analytical and numerical applications. *International Journal of Solids and Structures*. 2007. Vol. 44, no. 18–19, pp. 5930–5952. ISSN 00207683. DOI: 10.1016/j.ijsolstr.2007.02.005.

[19] LE CORVEC, V. and F. C. FILIPPOU, 2011. Enhanced 3D fiber beam-column element with warping

displacements. In: *ECCOMAS Thematic Conference - COMPDYN 2011: 3rd International Conference on Computational Methods in Structural Dynamics and Earthquake Engineering: An IACM Special Interest Conference, Programme*. 2011.

[20] FERRADI, M. K., X. CESPEDES and M. ARQUIER, 2013. A higher order beam finite element with warping eigenmodes. *Engineering Structures*. 2013. Vol. 46, pp. 748–762. ISSN 01410296. DOI: 10.1016/j.engstruct.2012.07.038.

[21] DIKAROS, I. C. and E. J. SAPOUNTZAKIS, 2014. Nonuniform shear warping effect in the analysis of composite beams by BEM. *Engineering Structures*. 2014. Vol. 76, pp. 215–234. ISSN 01410296. DOI:10.1016/j.engstruct.2014.07.009.

[22] TRAN, D. B., J. NAVRÁTIL and M. ČERMÁK, 2021. An efficiency method for assessment of shear stress in prismatic beams with arbitrary cross-sections. *Sustainability (Switzerland)*. 2021. Vol. 13, no. 2, pp. 1–20. ISSN 20711050. DOI: 10.3390/su13020687.

[23] WAGNER, W. and F. GRUTTMANN, 2002. A displacement method for the analysis of flexural shear stresses in thin-walled isotropic composite beams. *Computers and Structures*. 2002. Vol. 80, no. 24, pp. 1843–1851. ISSN 00457949. DOI: 10.1016/S0045-7949(02)00223-7.

[24] ÖCHSNER, A. and M. MERKEL, 2013. *One-Dimensional Finite Elements*. Springer. ISBN 978-3-319-75144-3. DOI: 10.1007/978-3-319-75145.

[25] OÑATE, E., 2013. *Structural analysis with the finite element method. Linear statics: volume 2: beams, plates and shells*. Springer Science & Business Media. ISBN 978-1-4020-8742-4.¨

[26] Available online: https://www.csiamerica.com/products (accessed on 05 December 2021).